Modelling of friction stir welding and its influence on the structural behaviour of aluminium stiffened panels

Modelling of friction stir welding and its influence on the structural behaviour of aluminium stiffened panels

R.M.F. Paulo[1], F. Rubino[2], R.A.F. Valente[3], F. Teixeira-Dias[4], P. Carlone[5]

[1] *School of Mechanical and Aerospace, Queen's University Belfast, United Kingdom*
[2]*Department of Chemical, Materials and Production Engineering, University of Naples Federico II, Italy*
[3]*Center for Mechanical Technology and Automation, Department of Mechanical Engineering, University of Aveiro, Portugal*
[4]*Institute for Infrastructure and Environment, School of Engineering, The University of Edinburgh, United Kingdom*
[5]*Department of Industrial Engineering, University of Salerno, Italy*
*Corresponding author: R.A.F. Valente; email address: robertt@ua.pt

Abstract

This work deals with the modelling and numerical simulation of aluminium stiffened panels, assembled by means of friction stir welding (FSW) operations, and subjected to compressive loads that can catastrophically induce buckling (global or local) unstable modes and, subsequently, overall failure. Due to their geometrical complexity, added to localized thermo-mechanical effects that typically come from joining by welding, approximation methods such as the Finite Element Method are typically used in such nonlinear analyses, having proved to be useful to designers focused on the prediction of the behaviour (before and post buckling) of such structures. Being grounded on previous contributions from the authors, the present paper aims to bring a number of innovative aspects to the current state of the art by considering in the developed models the simultaneous influence of residual stress fields, material softening effects and geometrical imperfections. Doing so, it is possible to infer about the singular and combined influence of these effects in the overall structural performance of stiffened panels, building up a useful and comprehensive methodology for design stages.

Keywords:

Stiffened panels; Friction stir welding; Buckling; Material softening; Distortion; Residual stresses.

1. Introduction

Friction stir welding was widely used in industry as replacement for fusion welding especially in case of hard-to-weld metals, such as aluminum alloys, eliminating the issues related to the solidification of the melt metal and reducing distortions and residual stresses. FSW was also extended to weld structures consisting of sheets with stiffeners, like skin-stringer fuselage and other aircraft components [1,2], replacing the extruded panels or the riveted constructions. Published literature indicates two main configurations to obtain FSW skin-stiffener joining: overlap joint [1,3] and T-joint [4,5]. The first method consists in welding in lap joint configuration an extruded profile, typically having L- or Z-shaped cross section, on a flat sheet. The method proved to be able to produce sound joint with limited degradation of the material base properties. However, the fabricated structures are sensitive to the weld defects (especially kissing bond defect) under T-pull load conditions [1,3]. In the FSW of T-joints, the rotating tool, specifically designed for this type of weld, is inserted on the external surface of the skin [5], and then the tool is moved along the joint; the skin and the stringer are clamped in properly designed fixture to avoid any movement during the welding. Recently, the TWI has also developed a novel technique, called Stationary Shoulder Friction Stir Welding (SSFSW), consisting in a rotating pin mounted on a non-rotating shaped shoulder to produce "T" and corner welds. The tool is inserted in the corner between the skin and the stringer, obtaining sound joints with a reduced clamping fixture [6].

The spread of FSW process in the high-end sectors is associated with the knowledge on the connections between the welding process parameters, the properties of the obtained joints and the effects of the welding on the performance of the structures [4,7]. The proposed work is part of a larger research, which aims to achieve an understanding of the effects of FSW process on the buckling behavior of the FSWelded stiffened panels through the numerical simulation of the FSW process, along with its post-weld effects, and of the longitudinal compression.

Indeed, structural analyses of stiffened panels under compressive loads involve issues that, globally, cannot be properly accounted for using analytical or empirical methods. Among these complexities are, for instance, material nonlinearities, different boundary conditions and unexpected geometrical distortions, considering a large range of panels' geometries

available in the market and their inherent slenderness. In addition, welding processes can be responsible for additional imperfections that may affect the structural efficiency of these panels, for example, material softening and the build-up of residual stresses [8].

The residual stresses in FSW process arise from the heating-cooling cycles dictated by the tool movement along the weld line and the alterations in the material properties due to the heat and mechanical action of the tool [9–12]. Their evaluation is paramount to assess the performance of welded panels, either simple flat parts either stiffened panel. Destructive (such as sectioning techniques and contour method), semi-destructive (like hole-drilling and deep-hole techniques) as well as non-destructive methods (e.g. X-ray diffraction method) are currently employed to measure the residual stresses. From these analyses, researchers observed that the distribution and the magnitude of residual stresses are strictly dependent on geometrical (like tool shape and dimensions, tool positioning, fixing supports) and technological parameters (especially tool rotating speed and feed rate) [9,13–15].

The defects from FSW process are mainly related to the formation of voids inside the weld bead [16] the "kissing bond" that occur when lack of atomic bonds between two surfaces generated by the flow of stirred material [17] as well as low surface quality [18–20]. These defects may have detrimental effect on the strength and fatigue life of the weld. The geometrical imperfections, that also can influence the strength of FSWelded structures, are mainly due to a differential on plastic strains between the affected zones of the weld during the FSW and the presence of residual stresses. [21,22].

Numerical analysis of FSW process was addressed as useful tool to better understand the materials flow, stress, strains and temperatures fields during the friction stir welding, the influence of the process parameters on the performance of the fabricated structures, and to predict the effects of the welding, including the formation of residual stresses and modifications of materials properties, on the behavior of the stiffened panels.

In the last decades, different approaches were proposed to deal with the complexities of the FSW process deriving from the interdependence of structural and thermal phenomena. The efforts paid by many researchers were mainly directed to the modelling of material properties

[23], the definition of the mechanical and thermal interaction between the tool and the workpiece [24–28]. The modelling of evolution of material properties during the welding process has been directed to the evaluation of suitable constitutive laws that account for the dependence of the material properties on the strain rate and temperature. The first models used are based on the Zener-Hollomon equation developed by [29,30] and on the Johnson Cook plasticity model [31], followed by Buffa [32], Zhang and Chen [24], and Huertier [33], which proposed multiplicative and exponential path-independent laws. The heat generation in FSW process is mainly related to the thermomechanical interaction between the rotating tool and the workpiece [24]. The first models to describe the frictional forces (i.e. the shear stress) between tool surfaces and the workpiece during FSW process were based on the Coulomb's contact law. The proposed models implied a coefficient of friction that can be constant [34–36] or a function of the temperature [25], or of the slip rate [26,27]. Other authors [28,32,37] proposed a shear friction model where the shear stress is function of the shear strength of the material. Besides that, outstanding research activity was devoted to develop an appropriate modelling method able to deal with the large deformation and non-linearity involved in the FSW process, as testify by the published literature. These methods are mainly based on Lagrangian analysis[28,38–44], Eulerian analysis [45–47], and on the use of hybrid methods, Arbitrary Lagrangian and Eulerian (ALE) analysis [36], and coupled Eulerian-Lagrangian analysis (CEL) [48,49].

Due to these combined complexities, the use of software based on the Finite Element Method proves useful and necessary, as widely explored by different authors in the literature. Software packages such as Abaqus [50–54], ANSYS [55–57], LS-DYNA [58], ULSAS and MSC Marc [58] are some examples of consolidated alternatives, to cite but a few, in trying to accurately predict the structural behaviour of these reinforced structures.

In their previous works some of the authors proposed a method based on finite element model using shell elements to predict the residual stresses, geometrical imperfection and materials softening induced by the welding process [59,60]. Details about the approaches adopted and the assumptions to properly account for initial geometrical imperfections into the numerical simulation models of stiffened panels and an overview of the state-of-the-art

can be found in the recent works from the author [59,60]. The findings of these works are used as input for the model proposed in the present manuscript.

Besides geometrical imperfections, the effect of other phenomena resulting from the welding process involved in the manufacturing of stiffened panels must also be included into the model. These phenomena include nonlinear effects coming from material softening as well as residual stresses. One way of accounting for material softening effects coming from welding processes into the numerical model is, for instance, considering a pre-defined zone (a band along the weld line, or the heat affected zone – HAZ – itself [61]) where the material has a lower yield stress compared to the base material [1,50,55,56,58,62–67]. These studies have pointed out a reduction in the collapse load under compressive loads with the increase of the width of the affected zone, corresponding to a reduction of yield stress values. Not so explored, on the other hand, is the influence of softened material zones in the overall structural behaviour of the stiffened structures [56,68].

One way to numerically account for the residual stresses coming from welding process is to create a preliminary stage, before the compression of the panel is developed, where residual stresses are introduced into the model (that is, the structure in no longer in equilibrium) and proceeding with a numerical analysis to re-establish an equilibrated, neutral, state, and using a minimum amount of boundary conditions just to prevent rigid body effects. This preliminary stage will thus lead to distortions of the initial geometry and changes in the induced stress field, which now part of the model that will be used for subsequent simulations [1,68].

In the present work, the buckling behaviour of stiffened panels welded by FSW is numerically analysed. The innovative character of the paper relies on the consideration of, simultaneously, (i) residual stress fields, (ii) material softening effects, and (iii) geometrical imperfections being added to the numerical simulation models, in order to properly account for welding effects in real components. The present study and paper consolidate and expand, therefore, the preliminary studies from the authors in the field of friction stir welded aluminium panels, as presented in the recent references [59,60].

2. Model description for the numerical simulations

2.1 General aspects

The stiffened panels considered in the present work, subjected to compressive loading cases, presents three different cross-section geometries (Figure 1). The stiffened T-panel is based on the initial work of Yoon et al. [50] (and more recently studied by the authors in references [59,60]) and presents a 4 mm thickness on the base plate. The other two panel geometries (B45 and B60) are variations of the previous one, now with a blade stiffener dimensions of 45 and 60 mm. The red line shown in the cross sections represent the reference mid-thickness plane for build the shell elements used to model the panels [59,60].

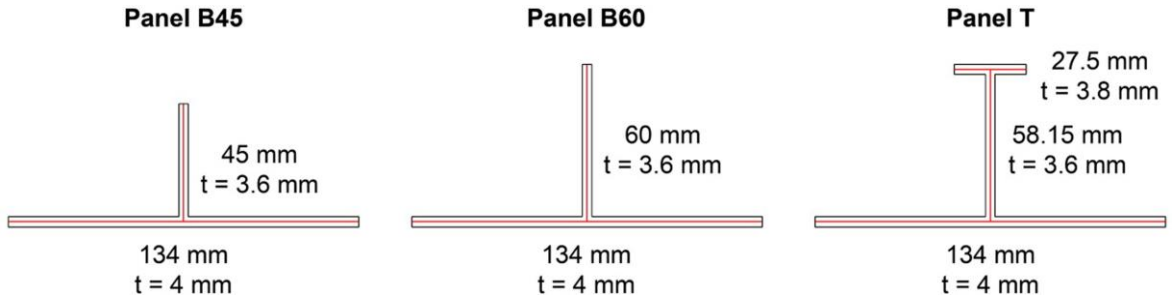

Figure 1: Cross-section and dimensions of the stiffened panels adopted in the present study, following references [59,60].

Stiffened panels were welded along the right edge of the skin (as highlighted in figure 2). Therefore, findings from previous researches of the authors [59], regarding residual stress, strength of weld as well as geometrical imperfections observed in FSWelded butt joint can be extended to the present work. The single stiffened panel could be considered as obtained by extrusion process; therefore, the properties of pristine alloy have been assigned to it. FSW analyses were preliminary performed on panels with length of 600 mm and 750 mm. Nonetheless, the structural numerical analyses will focus only on the middle part of the 750 mm-long panel (corresponding to an effective length of 600 mm). This choice intends to avoid localization effects due to the beginning and end of the weld located close to the transverse edge [59,60]. Previous results from FSW numerical analysis on the three configurations allowed to estimate the stress distribution, the materials softening and deformed shapes in the panels [59], while the influence of different modelling approaches

on the predicted structural stability and performance of the panels was covered in [60]. Regarding the modelling and numerical simulation choices, the adopted finite element formulation corresponds to a reduced integration shell type model (finite element code S4R in Abaqus software), with a similar approach to the areas affected by welding (S4RT finite element type). From the previous works of the authors, these choices have shown good performance in terms of accuracy/computational time ratio when compared to alternative shell formulations. For both shell formulations, 5 integration points were considered across the thickness direction, which is the default option available in Abaqus FE software. Material properties considered in the present paper are those of aluminium alloy AA2024-T3. Details can be found in the published literature [69–71].

2.2 Definition of boundary conditions

The mechanical boundary conditions used during the compression stage are schematically shown in Figure , following a previous work from the authors [60]. Symmetry conditions were applied to nodes along the weld line as well as along the edge opposite to the weld line. These definitions allow simulating a larger panel with a weld join per every two stiffeners' section. However, and as a consequence of this choice, the model is capable of only reproducing the periodic buckling modes that can appear in a single section. This is however not a limitation, since those buckling shapes are those that are typically expected in these cases [59,60].

Two rigid walls were defined in each one of the transverse edges of the panels, using connector elements with 2 nodes (CONN3D2 element type in Abaqus), in order to restrain relative displacements between them. In one of these sections, clamped boundary conditions were applied (*encastre* area in Figure 2), while in the opposite one displacement along the loading direction (*Oz*) was allowed. At this section, a load or displacement (depending on the solving methodology) can be imposed along *Oz* direction in order to induce longitudinal compression in the model of panels. For the panels with 750 mm of length, the rigid walls were defined using the nodes placed at 75 mm from each one of the transverse edges of the panel, therefore creating an effective length of 600 mm, as mentioned before. Details on the different modelling strategies tested, regarding the unstable load/displacement longitudinal compression path following with Abaqus, can be found in [60].

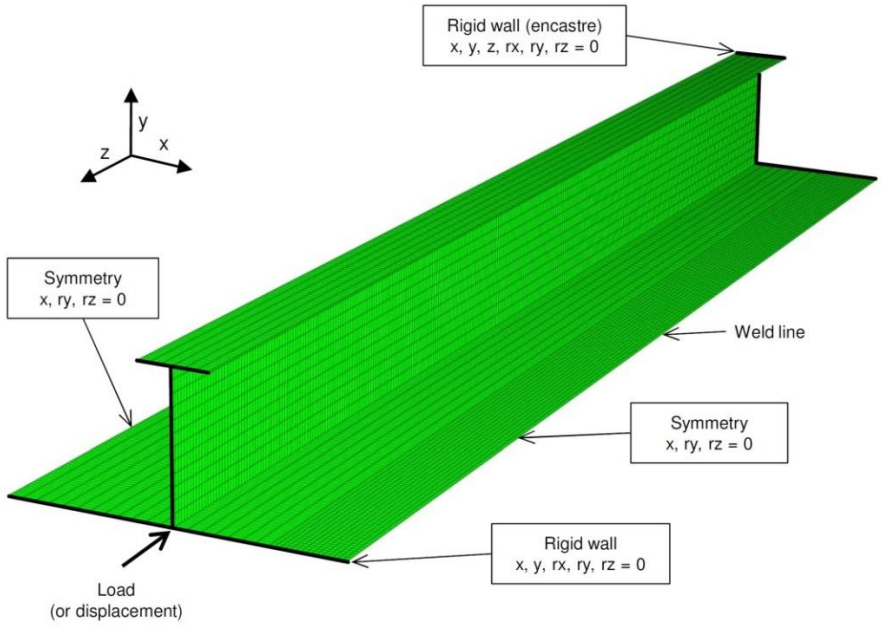

Figure 2: Mechanical boundary conditions for the compressive structural analyses [60].

3. Modelling of the FSW effects stiffened panels

In this section, the procedures carried out for the numerical modelling of the friction stir welding (FSW) effects on the chosen stiffened panels (B45, B60 and T profiles) will be described in detail.

The FSW influence will be taking into account in the finite element models by means of considering three different approaches: (i) the use of geometrical imperfections (IMP, in the following), necessary to trigger buckling effects in the numerical simulation models; (ii) the modelling of residual stress effects (RS, in the following); (iii) material softening effects (SOFT, in the following). Different combinations of such effects, and their influence on the overall numerical simulation models for each panel will be considered. From these three sources of imperfections into the model, special consideration will be given to properly model the residual stresses and the material softening effects, leading to different combination of welding conditions. Regarding material softening effects, two particular distributions were tested: (i) the scenario of *softening before ageing* (designated by SOFT60 in the following, for a minimum yield stress equals to 60% of the base material's); and (ii)

the scenario of *softening after the ageing process* (designated by SOFT75, for a minimum yield stress equals to 75% of the base material's).

The effects of the FSW process were modelled using two different methodologies. The first one consisted in importing into the model the welding effects from a previously performed FSW numerical analyses on the 600 and 750 mm panels, including or neglecting the residual stresses, prior to the application of the compressive load, as described in [59]. The analyses, including residual stresses, were carried out first neglecting the ageing of the material (SOFT60), and secondly considering the material natural ageing (SOFT75). In the analyses without the residual stress field the geometrical imperfections were imposed as displacements in the original mesh (using the *IMPERFECTION command in Abaqus software [72]). The material softening was imposed using the intended properties: base material (no softening), after welding (SOFT60) or after natural ageing (SOFT75). Material softening distributions was derived from previous FSW numerical simulations [59].

The second methodology was a simplified one and previously described in the literature [1,68,73], and consists of adopting welding effects (magnitude and location) also coming from numerical analyses of FSW [59], but now added to the numerical model by means of using simplified distributions. This approach assumes a perfectly plastic behaviour, followed by including separately the work hardening effects. For sake of clarity, details about the simplified methodology as well as the softened material distributions and magnitudes are reported in Appendix A.

All possible combinations are listed in Table 1 for the different models with the distinct welding effects. It should be mentioned that the analyses performed with the material properties before ageing (SOFT60) have no relevance in terms of practical application. However, they can be useful in understanding the effects of softening effects on the panel behaviour.

Table 1: Summary of the models and combinations of FSW effects tested and nomenclature used

Models tested (FSW effects origin and model details)	FSW simulation (600 mm panels) FSW simulation (750 mm panels) Simplified method (described in Appendix A) Simplified method including work hardening
Combinations of FSW effects tested	IMP IMP + SOFT75 IMP + SOFT60 IMP + RS IMP + SOFT75 + RS IMP + SOFT60 + RS

Nomenclature:
IMP – Geometrical imperfections
SOFT75 - Softened material in the FSW zone with yield stress equal to 75% of the base material
SOFT60 - Softened material in the FSW zone with yield stress equal to 60% of the base material
RS – Residual stresses

The simplified methodology used to include the FSW effects has led to symmetry of the displacements and stress fields regarding a plane corresponding to the panel mid-length. Therefore, and taking into account that the material distribution (in all cases) is also symmetric, the model shows as a consequence a full symmetric behaviour respecting the mentioned plane. This assumption can have implications on the structural buckling, since with the present models only symmetrical buckling modes can be obtained after longitudinal compression. Although the study of unsymmetrical (and local) buckling modes is out of the scope of the present paper, the overall modelling methodology can be extended to those situations by alleviating the symmetry boundary conditions in the setup of the modelling stage.

4. Results and discussion

4.1 General considerations

In the following, and regarding the influence of welding effects on the panels, three distinct scenarios will be compared in order to assess the consequences of the adopted modelling strategies:

(i) modelling 600 mm panels *vs.* 750 mm panels, to infer about the impact of the extremities (border) effects on the panel strength;

(ii) the use of a perfectly plastic model *vs.* the use of work hardening laws;

(iii) the use of effects coming from FSW numerical analyses (more realistic) *vs.* the simplified modelling of these factors.

These effects will be discussed below in separate subsections. The results regarding the collapse loads, as coming from the modelling and numerical simulation of the imposed compressive load/displacements, are shown in Table 2. In order to properly compare the collapse loads for different panels, these are separately represented in Figure 3. Also for the sake of comparison between different stiffened panels, Figure 3 presents values of the *normalized collapse loads*, that is the value of the collapse load for each panel, as coming from the numerical simulations, divided by the respective collapse load coming from models only including geometrical imperfections (IMP), therefore not being influenced by residual stresses or softening effects.

Table 2: Collapse load predictions for compression analyses including different combination of FSW effects.

		Collapse loads for distinct FSW effects combinations (kN)					
FSW effects origin (model details)	Panel	IMP	IMP SOFT75	IMP SOFT60	IMP RS	IMP SOFT75 RS	IMP SOFT60 RS
FSW simulation (600 mm panels)	B45	180.15	178.38	177.31	180.05	179.63	178.98
	B60	184.01	182.33	181.05	182.94	182.51	181.94
	T	256.38	251.53	254.36	245.28	243.06	241.76
FSW simulation (750 mm panels)	B45	180.04	178.32	177.41	180.28	179.73	179.14
	B60	183.96	182.26	180.99	183.02	182.53	181.95
	T	256.93	252.21	254.71	247.59	243.46	242.11
Simplified modelling	B45	181.57	179.99	178.85	181.38	181.12	180.61
	B60	185.35	184.06	183.14	185.53	185.36	185.03
	T	235.33	239.95	238.79	243.68	242.77	241.59
Simplified modelling (including work hardening)	B45	181.74	180.22	179.64	181.50	181.25	180.77
	B60	185.50	184.20	183.32	185.72	185.51	185.17
	T	235.92	240.94	239.43	244.14	243.23	242.11

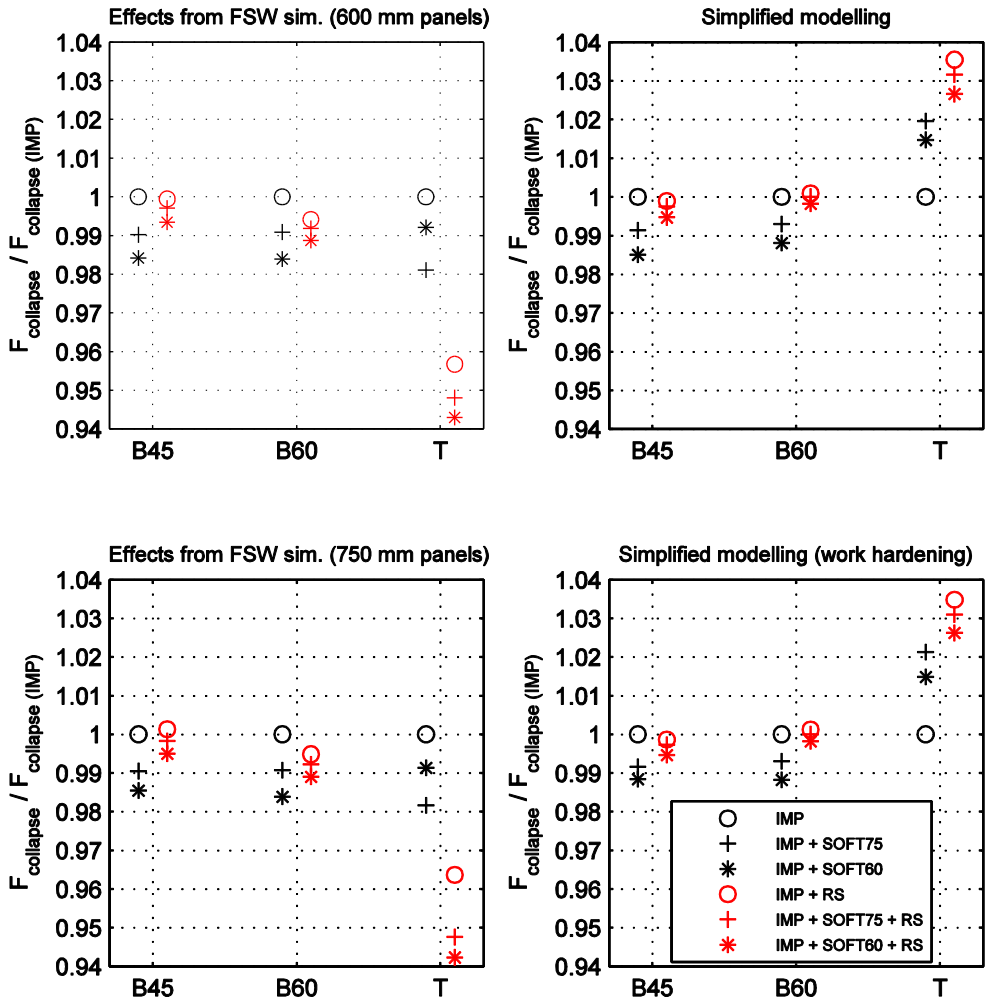

Figure 3: Collapse load magnitude for the panel compression analyses, normalized to the result from the model with geometrical imperfections only (IMP), for each stiffened panel profile.

On the other hand, *Figure* presents the same results but now normalized with respect to the yield load of each panel, i.e. the load that each panel can withstand before developing plastic deformation in the absence of buckling effects. This ratio between the collapse load and the yield load is often taken into consideration in research works involving stiffened panels analyses, since it can provide an estimation of the strength efficiency for each panel.

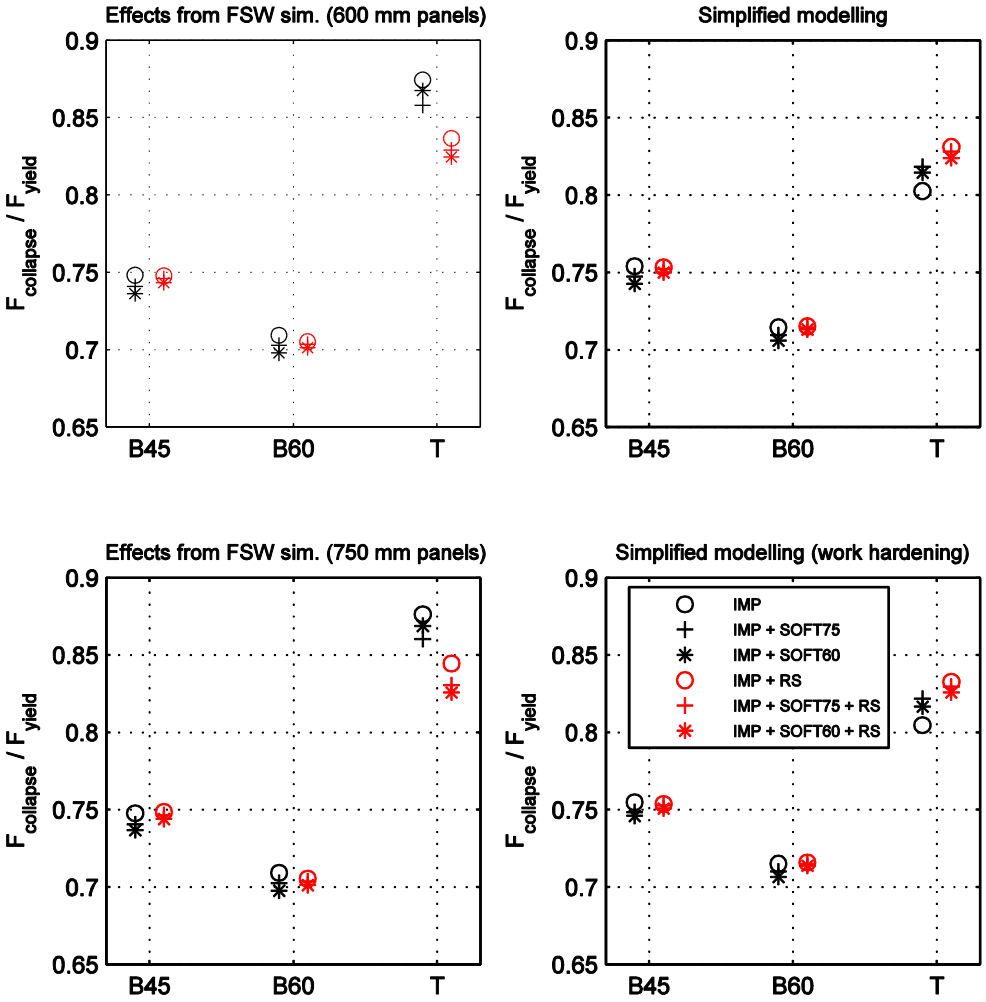

Figure 4: Collapse load magnitude for the panel compression analyses, normalized to the yield load magnitude of each panel.

From the figures and table before, clear differences between panel T configuration and the blade stiffened ones (B45 and B60) can be observed, regarding the load/end shortening curves and collapse loads. The first difference is that the ratio between the collapse load and the yield load is significantly higher in panel T, with a minimum ratio value of 0.805 (Figure 4). On the other hand, the second difference points to the apparent higher sensitivity of panel T, with a higher range of variation of the collapse load as coming from the different analyses.

Appendix B presents a summary of the buckling modes for the analysed stiffened panels, in order to provide an overview of the deformed configurations as coming from the numerical simulation analyses, and the influence of different decisions regarding the modelling of imperfections as coming from FSW operations. This is of interest since complete FSW

effects model and simplified model sometimes can lead to distinct evolution of buckling shapes through the compressive loading process.

4.2 Influence of the longitudinal extremities welding effects

The results using the 600 mm and the 750 mm panels are not significantly different, and both led to the same conclusions concerning the welding effects. The maximum variations obtained, comparing models with combination of the same welding effects, are 0.13% and 0.04%, for the panels B45 and B60, respectively. For panel T, more sensitive to modelling variations, the differences are lower than 0.27%, except for the model with IMP + RS, that shows a variation of 0.93% due to a slight difference in the buckling evolution just before the collapse load (Table 2), with all variations being randomly negative or positive. The slight differences in the initial geometrical distortion in the panels with different lengths and the deviations associated with the FEA can justify these variations. There are no evidences that effects close to the transverse edges, related to the softening of the material or with the residual, have any influence in the collapse load of the panels.

4.3 Influence of using work hardening properties instead of a perfectly plastic definition

Collapse load showed to be slightly influenced by the use of work hardening properties instead of a perfectly plastic model (as coming from the FSW numerical analyses). Models including work hardening properties, as expected, attained higher values of collapse load for all tested configurations. For panels B45 and B60, the variations in the collapse loads are smaller than 0.13%, except for the particular case of panel B45 with IMP + SOFT60, with a variation of 0.44%. For panel T, the differences are generally higher (between 0.19% and 0.41%), which can be a consequence of the higher ratio between the collapse load and the yield load, involving a higher plastic deformation at the moment of collapse for these panels and, therefore, a higher influence of the plastic properties of the material.

Therefore, the correct definition of the plastic deformation properties may have an important effect in the accuracy of results, especially in high efficiency panels (with a high collapse load/yield load ratio). Nonetheless, both of the material properties modelled (with and

without work hardening) can lead to similar conclusions in terms of the influence of welding effects on the collapse load, as can be seen from the results in Figure 3.

4.4 Effects of residual stress field

A primary effect of the residual stresses on the behaviour of the welded panels consisted in a delay of the first mode-change compared to the equivalent panels without the residual stresses. This delay in the mode-change, in terms of end shortening, led to a higher load magnitude. This occurrence was observed for all sample except for the T panel.

The curves from models with IMP and with IMP + RS effects are represented in Figure 5 (a), focusing on the zone associated with the mode-change. The deformed shapes corresponding to the points marked in the curve are depicted in (Figure 5(b)), which show that the deformed shape with a single global curve evolves earlier to three half waves on the model without the residual stresses. This is also evident on the results presented in Figure 6, that shows the evolution of the out-of-plane displacement in three points located on the mid-length section of the panel. In all curves it is noticeable that the out-of-plane displacement has a later increase (in absolute terms) in the panel with residual stresses, concerning the zone with an end shortening between 1 and 1.3 mm. The evolution of the longitudinal stresses in the same three points is represented in Figure 7 and it also shows a delayed evolution associated with the presence of residual stresses. Particularly in this case, it is important to verify the bifurcation of the curves corresponding to the top and bottom of the base plate, and right and left in the stiffener. This bifurcation corresponds to a mode-change pattern and is shown to occur later for the model including the residual stress effects.

(a)

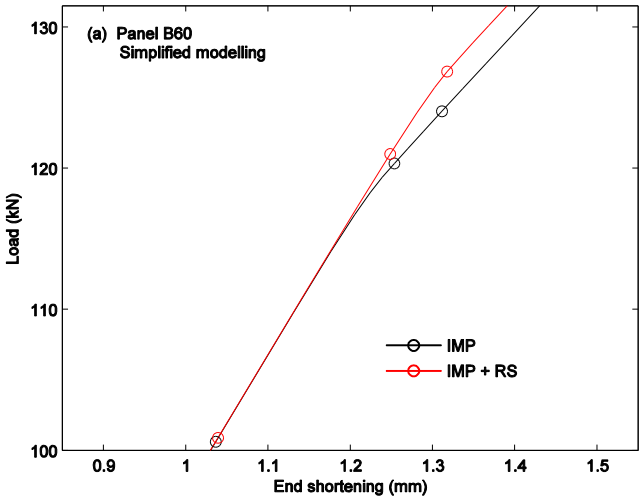

(b)

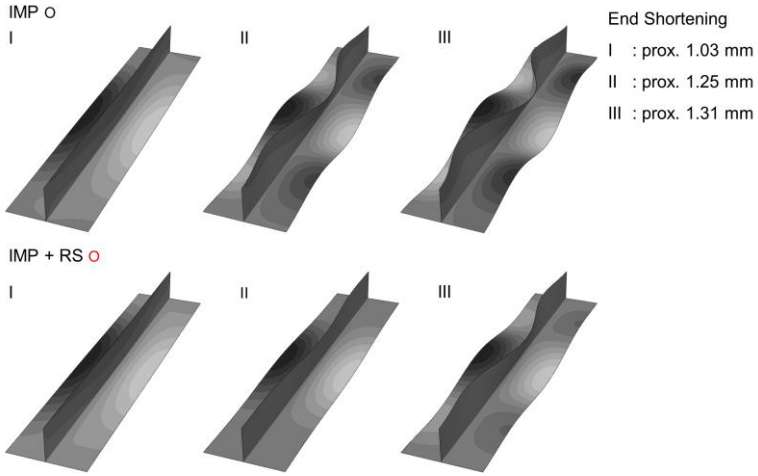

Figure 5: Mode-change in the panel B60, including the simplified modelling of the welding effects (i.e. IMP, for model accounting only for geometrical imperfections, IMP+RS, for model accounting for geometrical imperfections and residual stress): (a) curve load/end shortening;(b) corresponding buckling shapes at different displacements of stiffened panel end: proximally 1.04 (I),1.25 (II) and 1.31 mm (III). The displacements are amplified 15 times along Ox and Oy.

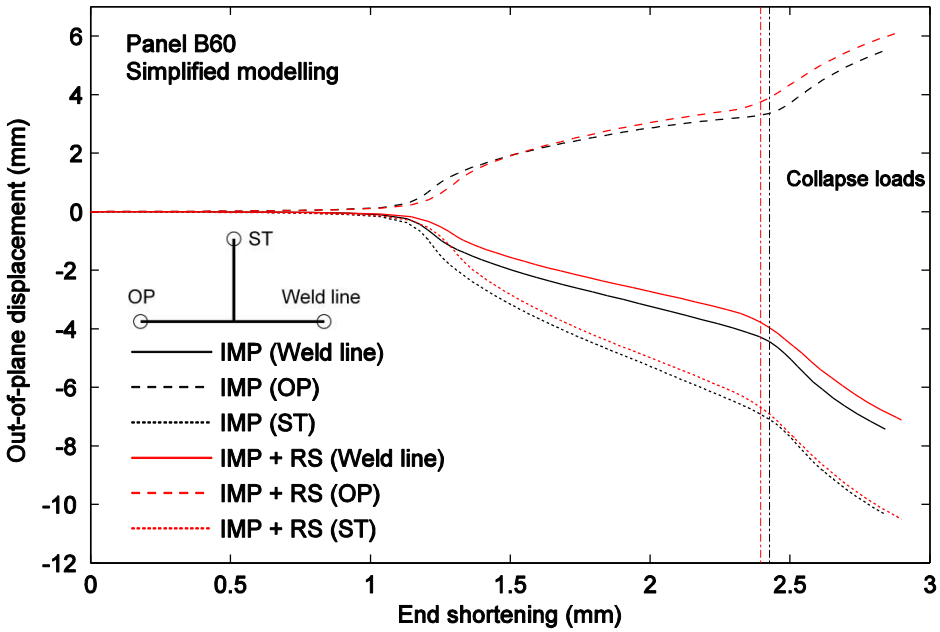

Figure 6: Out-of-plane displacement variation in three points located at mid-length of the panel B60, including the simplified modelling of the welding effects.

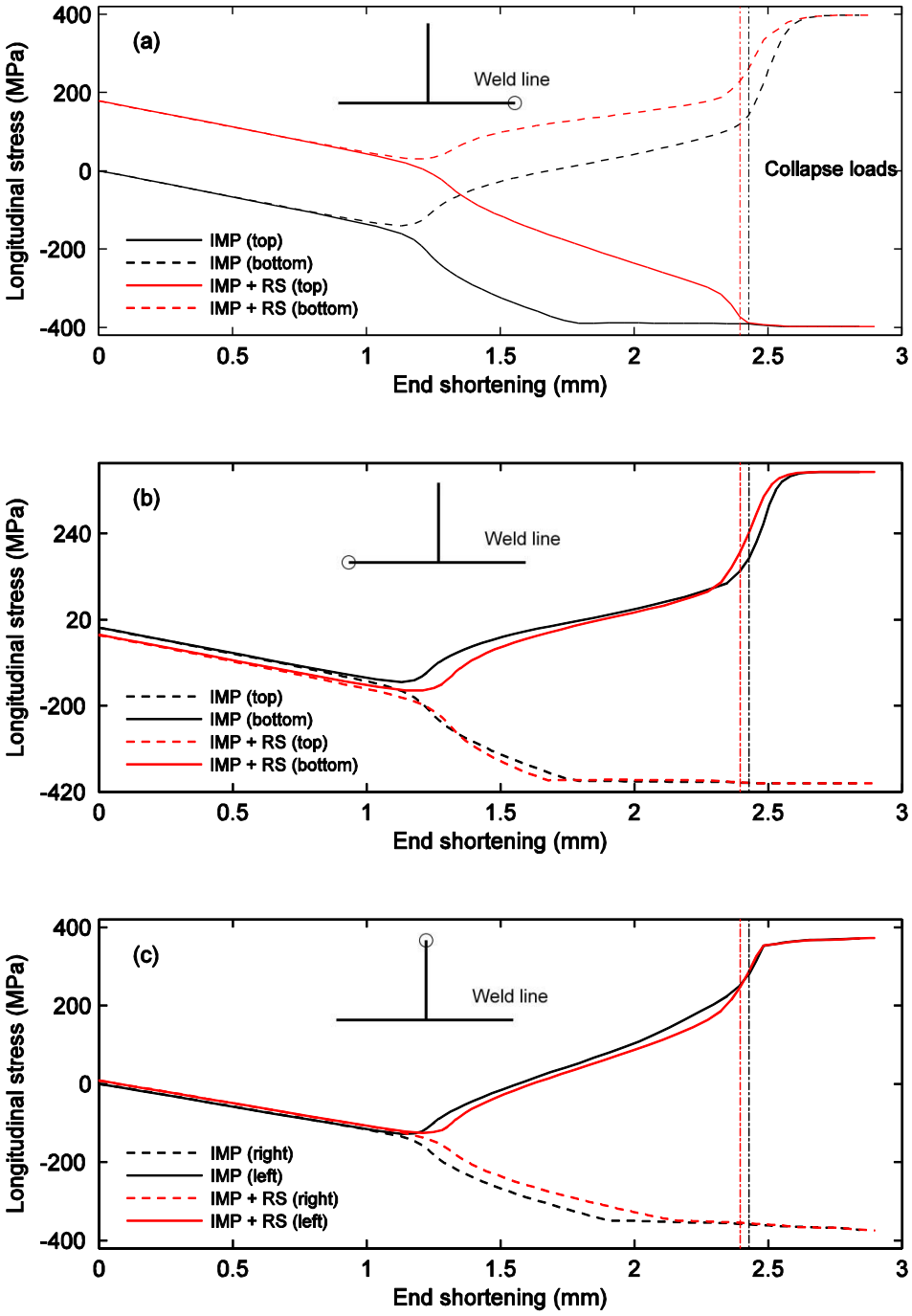

Figure 7: Longitudinal stress variation in three points located at mid-length of panel B60, including the simplified modelling of the welding effects: (a) in the weld line, (b) on the edge opposite to the weld line, and (c) at the top of the stiffener.

Including the FSW effects into the models for B45 and B60 panels resulted in a mode changing behaviour that seemed to occur later (for higher end shortening and higher load), although being more abrupt when compared to the simplified modelling. This is related to the shape and magnitude of the initial imperfection. The existence of initial geometrical imperfections (single half wave curvature) with higher magnitude delayed the formation of the three half waves buckling mode, because these involved the displacement of some parts of the panels to the opposite side in terms of out-of-plane position.

4.5 Influence of material softening

As far the effect of material softening on the panel behaviour, looking at the results for panels B45 and B60, the collapse load decreased with the decrease in the yield stress properties in the weld affected zone both in the models with and without residual stresses. This effect can also be observed in all results of T panel that exhibited similar collapse shapes.

The simplified modelling (see Appendix A) of the welding effects on panel B60 is again used as example to give an overall explanation of the softening effect in the panel behaviour. The differences in the behaviour between the panel with only geometrical imperfections effects (IMP) and the ones including also the materials softening (IMP + SOFT60 and IMP + SOFT75) is related to the plastic strain in the welded zone, which begins earlier for panels with lower yield stress in the affected zone. Results in Figure 8(a) show the stress magnitude when the panel just with initial geometrical imperfections (IMP) reaches an end shortening of 1.6 mm.

It can be seen that the stress levels are higher at the centre of the base plate (close to the weld line and opposite edge) and large enough to initiate plastic deformation if the material's yield stress was the one of the affected materials in the welded zone. For the same model, Figure 8(b) represents the stress magnitude at the moment of collapse, while Figure 9(a) shows the associated equivalent plastic strain. Comparing this plastic strain with the one of the model with material softening (IMP + SOFT60), represented in Figure 9(b), higher deformations can be observed (at the moment of collapse) close to the weld line in the model with the

softened material. The earlier and higher plastic deformation leads to a lower collapse load of the panels with softened material.

The observed effects of the softened material on the panel behaviour, without the presence of the residual stress field, is also verified when the residual stresses are considered. Nonetheless, in the presence of the residual stresses, the impact on the collapse load magnitude is lower, as can be observed in Figure 3 and Figure 4. Indeed, according to the result from the analysis of panel B60 with simplified modelling of the welding effects, it is possible to verify that the difference between the models with IMP and with IMP + SOFT60 is 1.19%, while the difference between the models with IMP + RS and with IMP + SOFT60 + RS is only 0.19%.

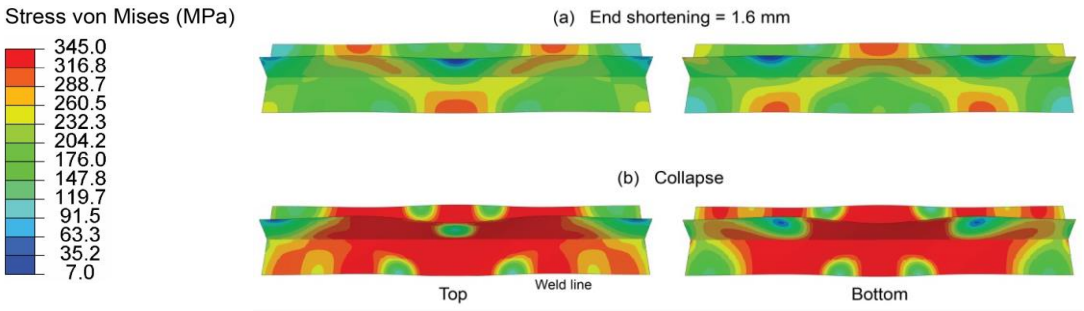

Figure 8: Von Mises stress distribution in panel B60 (top and bottom of the plates) including only the geometrical imperfections (IMP) obtained using the simplified modelling of the welding effects: (a) at end shortening equal to 1.6 mm and (b) at collapse.

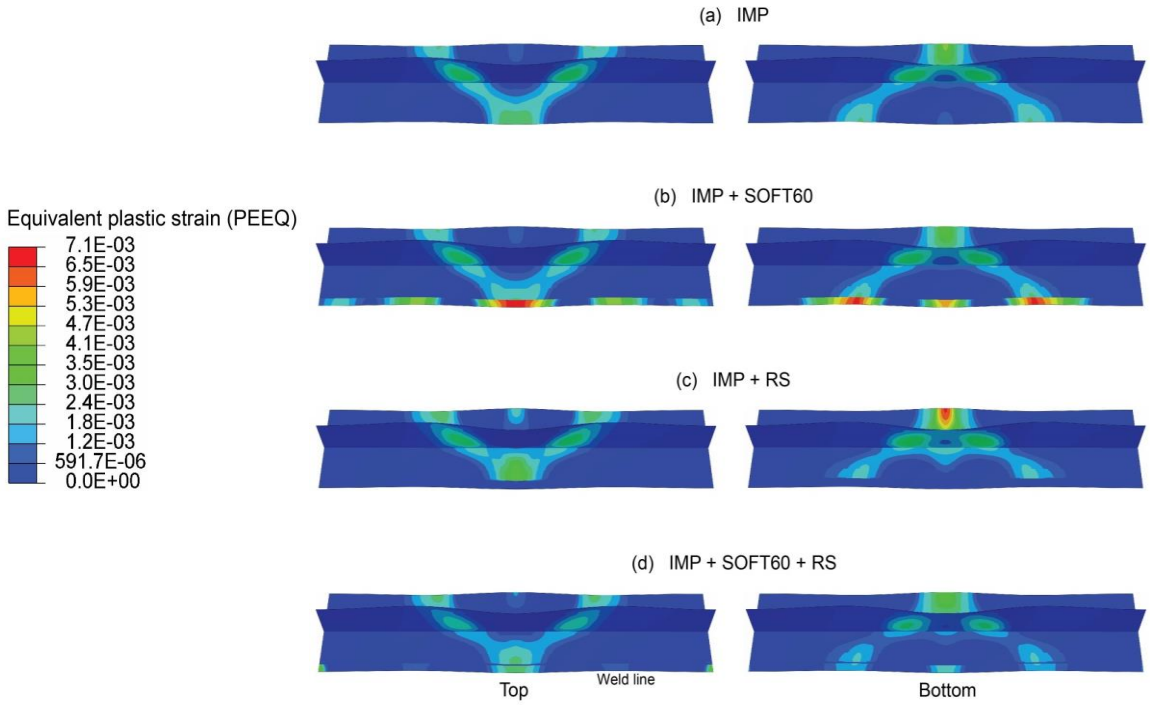

Figure 9: Plastic strain in panel B60 (top and bottom of the plates) at collapse including the simplified modelling of the welding effects with different combinations: (a) IMP, (b) IMP + SOFT60, (c) IMP + RS and (d) IMP + SOFT60 + RS.

Results from the simplified modelling of the welding effects of panel B60 will help to explain the effect of the residual stress field on the collapse load. Comparing the plastic strain at the moment of the collapse, in the panels with base material properties, without and with residual stress (Figure 9(a) and (c), respectively), it is possible to observe that the existence of a zone with tensile stress (close to the weld line) reduced the plastic strain to zero close to the weld line (Figure 9(c)). Close to the edge opposite to the weld line, the plastic strain is higher in the model with residual stresses. The reason for this is that when the panel is loaded in compression the stress along the longitudinal direction decreases, as represented in Figure 7, until the buckling leads to a bifurcation in the stress path between the top and bottom of the metal sheet. Afterwards, in the concave zones the stress continues to decrease, while in the convex parts the longitudinal stress increases. It is important to mention that all the plastic strain at the moment of collapse happen due to compression. The initial tensile residual stress in the welded zone delays the increase of the compressive stress, as can be seen in Figure 7(a), avoiding plastic deformation at the moment of collapse.

On the contrary, in the opposite edge to the weld line, the existence of compressive stresses in the beginning slightly increases the compressive load in that zone, leading to an early plastic deformation and a higher magnitude at collapse. Nonetheless, in this case, the collapse load is similar in the two models (IMP and IMP + RS). In the presence of a zone with softened material, the residual stresses increase the collapse load (see Figure 3 and Figure 4). The existence of the softened zone (see Figure 9(b)) increases the plastic deformation close to the weld line. In the presence of residual stresses and softening, the existence of the tensile stress in the welded zone strongly reduces the plastic deformation in that part. At the same time, there is not a higher plastic deformation close to the opposite edge of the line, as can be seen in Figure 9(d), and the plastic deformation is similar to the one obtained with the model with geometrical imperfections only (see Figure 9(a)). Therefore, the presence of the residual stresses shows two effects on panels B45 and B60: it increases the collapse load in the presence of softened material and leads to a decrease of the impact of the softened material on the collapse load. The increase of the collapse load in panels with a HAZ, in the presence of the residual stresses, was also shown by Murphy et al. [68].

The outcomes obtained from the two chosen methodologies, FSW analyses and the simplified modelling approach, to account for welding effects can be compared. The initial geometrical imperfection adopted in each method is different. The one obtained in the simplified modelling (Appendix A), generated by the residual stress fields added to the model, have a lower maximum magnitude, since the typical V-shape in the transverse direction is reduced when compared to the deformed shape from the FSW simulation [59]. As previously observed, this difference influences the panels' behaviour in terms of the buckling evolution and collapse mode, as happens for panels B60 and T, with obvious impact on the collapse load. Furthermore, also in the presence of the same collapse mode, as happens for panel B45, different geometrical imperfections significantly affected the collapse load. The assessment of using different residual stress and softening distributions is hampered due to the dominance of the initial imperfections effect. Nonetheless, the results in general, and especially the ones obtained with panel B45, do not show evidence of significant differences using a detailed modelling of these welding effects from FSW simulation instead of a simplified one.

In terms of the panel design and application, the influence of the welding effects in terms of residual stress and softening can be assessed comparing the IMP models with the IMP + SOFT75 + RS (since the panel with softening after ageing and residual stresses is the one that can be used in a practical application). Table 3 presents the collapse load variation between these two models for the different panels. The welding effects softening together with residual stresses led to a slight decrease in the collapse load, in most cases, although the preponderance of the initial geometrical imperfection using the two methodologies proposed makes it difficult to perform a valid comparison.

Table 3: Variation of the collapse load.

FSW effects origin	Panel	Collapse load variation (%) (comparing the model with IMP + SOFT75 +RS with model with IMP)
FSW simulation (600 mm model)	B45	-0.29
	B60	-0.82
	T	-5.19
Simplified modelling	B45	-0.25
	B60	0.00
	T	3.16

5. Conclusions

The results coming from the modelling and numerical simulation of the compression of stiffened panels, by means of the Finite Element Method and using Abaqus software, allow to infer how distinct modelling choices in the preliminary stages and setup can impact the overall structural behaviour of aluminium stiffened panels assembled by friction stir welding operations.

In a summary way, it can be concluded that:

- distinct distributions of the welding effects close to the transverse edges were tested. and there is no evidence that either the differences in the residual stress distribution or in softened material distribution have noticeable influences on the final results;

- the use of work hardening properties (compared to the adoption of simple perfectly plastic relation) has led to an increase of the collapse load, which was more significant for panels with higher collapse load/yield load ratio, once the equivalent plastic strain levels were also higher in these cases;
- the use of two different methodologies to model the welding effects (effects from FSW simulations and the simplified modelling) has showed differences in the results mainly due to the use of different initial geometrical imperfections;
- the distinct modelling of the residual stress field and softened material did not show any impact on the results. Nonetheless, the detailed definition of the welding effects from the FSW simulation can be important in other studies such as, for example, fatigue analysis;
- a strong influence of the initial geometrical imperfections was observed on the panels' buckling modes and collapse loads; these imperfections also showing influence on the impact of the remaining welding effects;
- in panels with similar collapse mode, the existence of softened material in the welded zone led to a decrease on the collapse load.
- in panels with similar collapse mode, the presence of residual stress fields led to a delay in the first mode-change during loading. In addition, in the presence of softened material in the welded zone, the existence of the residual stress field led to an increase in the collapse load. In some cases, the presence of residual stresses or softened material has shown to also affect the buckling modes;
- considering the noticeable influence on the overall behaviour of the panels of initial geometrical imperfections, an additional set of analyses considering for the initial setup deformed shapes coming from eigenvalue (EV) analyses might be of interest to better assess the sensitivity of the panels regarding initial geometrical imperfections.

CRediT authorship contribution statement

R.M.F. Paulo: Visualization, Investigation, Writing- Original draft preparation, Writing- Reviewing and Editing; F. Rubino: Writing- Reviewing and Editing; R.A.F. Valente: Conceptualization, Methodology, Funding acquisition, Writing- Reviewing and Editing; F. Teixeira-Dias: Data curation; Validation. P. Carlone: Supervision, Writing- Reviewing and Editing.

Declaration of competing interest

None.

Acknowledgments

The authors wish to acknowledge the support given by *Fundação para a Ciência e a Tecnologia, Ministério da Ciência, Tecnologia e Ensino Superior*, Portugal, under grants PTDC/EME-PME/113835/2009 and SFRH/BD/82456/2011. The support from the Center for Mechanical Technology and Automation (TEMA), University of Aveiro, under projects UID/EMS/00481/2013-FCT and CENTRO-01-0145-FEDER-022083, is also acknowledged.

References

[1] A. Murphy, W. McCune, D. Quinn, M. Price, The characterisation of friction stir welding process effects on stiffened panel buckling performance, Thin-Walled Struct. 45 (2007) 339–351. https://doi.org/10.1016/j.tws.2007.02.007.

[2] B.. Christner, J.. McCoury, S. Higgins, Development and testing of friction stir welding (FSW) as a joining method for primary aircraft structure., in: Proc. 4th Int. Frict. Stir Weld. Symp., Park City, UT, USA, 14–16 May 2003, 2003: pp. 57–68.

[3] S. Ciliberto, A. Astarita, A. Squillace, FSW of T joints in overlap configuration: process optimization in joining dissimilar aluminium alloys for the aeronautic application, Surf. Interface Anal. 45 (2013) 1631–1637. https://doi.org/10.1002/sia.5214.

[4] L. Fratini, G. Buffa, L. Filice, F. Gagliardi, Friction Stir Welding of AA6082-T6 T-joints: Process Engineering and Performance Measurement, Proc. Inst. Mech. Eng.

Part B J. Eng. Manuf. 220 (2006) 669–676. https://doi.org/10.1243/09544054JEM327.

[5] L. Fratini, FSW of Lap and T-Joints, in: 2010: pp. 125–149. https://doi.org/10.1007/8611_2010_48.

[6] J. Martin, C. Stanhope, S. Gascoyne, Novel Techniques for Corner Joints Using Friction Stir Welding, in: TMS 2011 Annu. Meet. Exhib., San Diego, CA., USA. 27 Feb. - 3 Mar. 2011., 2011. https://www.twi-global.com/technical-knowledge/published-papers/novel-techniques-for-corner-joints-using-friction-stir-welding#ref3.

[7] A. Murphy, F. Lynch, M. Price, A. Gibson, Modified Stiffened Panel Analysis Methods for Laser Beam and Friction Stir Welded Aircraft Panels, Proc. Inst. Mech. Eng. Part G J. Aerosp. Eng. 220 (2006) 267–278. https://doi.org/10.1243/09544100JAERO51.

[8] D.M. Finch, F.M. Burdekin, Effects of welding residual stresses on significance of defects in various types of welded joint, Eng. Fract. Mech. 41 (1992) 721–735. https://doi.org/10.1016/0013-7944(92)90156-9.

[9] P. Carlone, G.S. Palazzo, Longitudinal Residual Stress Analysis in AA2024-T3 Friction Stir Welding, Open Mech. Eng. J. 7 (2013) 18–26. https://doi.org/10.2174/1874155X01307010018.

[10] A. Steuwer, M.J. Peel, P.J. Withers, Dissimilar friction stir welds in AA5083–AA6082: The effect of process parameters on residual stress, Mater. Sci. Eng. A. 441 (2006) 187–196. https://doi.org/10.1016/j.msea.2006.08.012.

[11] Z. Feng, X.-L. Wang, S.A. David, P.S. Sklad, Modelling of residual stresses and property distributions in friction stir welds of aluminium alloy 6061-T6, Sci. Technol. Weld. Join. 12 (2007) 348–356. https://doi.org/10.1179/174329307X197610.

[12] C. Liu, X. Yi, Residual stress measurement on AA6061-T6 aluminum alloy friction stir butt welds using contour method, Mater. Des. 46 (2013) 366–371. https://doi.org/10.1016/j.matdes.2012.10.030.

[13] A. Bastier, M.H. Maitournam, F. Roger, K. Dang Van, Modelling of the residual state of friction stir welded plates, J. Mater. Process. Technol. 200 (2008) 25–37. https://doi.org/10.1016/j.jmatprotec.2007.10.083.

[14] D.G. Richards, P.B. Prangnell, S.W. Williams, P.J. Withers, Global mechanical

tensioning for the management of residual stresses in welds, Mater. Sci. Eng. A. 489 (2008) 351–362. https://doi.org/10.1016/j.msea.2007.12.042.

[15] V. Richter-Trummer, E. Suzano, M. Beltrão, A. Roos, J.F. dos Santos, P.M.S.T. de Castro, Influence of the FSW clamping force on the final distortion and residual stress field, Mater. Sci. Eng. A. 538 (2012) 81–88. https://doi.org/10.1016/j.msea.2012.01.016.

[16] P.L. Threadgill, A.J. Leonard, H.R. Shercliff, P.J. Withers, Friction stir welding of aluminium alloys, Int. Mater. Rev. 54 (2009) 49–93. https://doi.org/10.1179/174328009X411136.

[17] A. Oosterkamp, L.D. Oosterkamp, A. Nordeide, "Kissing bond" phenomena in solid-state welds of aluminum alloys, Weld. J. (Miami, Fla). 83 (2004) 225-S. https://www.scopus.com/inward/record.uri?eid=2-s2.0-4043071189&partnerID=40&md5=d1db3b295f1cd00dfd97cfce2cd15f1f.

[18] R.S. Mishra, Z.Y. Ma, Friction stir welding and processing, Mater. Sci. Eng. R Reports. 50 (2005) 1–78. https://doi.org/10.1016/j.mser.2005.07.001.

[19] H. Bisadi, A. Tavakoli, M. Tour Sangsaraki, K. Tour Sangsaraki, The influences of rotational and welding speeds on microstructures and mechanical properties of friction stir welded Al5083 and commercially pure copper sheets lap joints, Mater. Des. 43 (2013) 80–88. https://doi.org/10.1016/j.matdes.2012.06.029.

[20] A. J, C. Gambaro, E. Lertora, P. M, M. Szkodo, Analysis of FSW welds made of aluminium alloy AW6082-T6, Arch. Mater. Sci. Eng. 28 (2007).

[21] D. Yan, A. Wu, J. Silvanus, Q. Shi, Predicting residual distortion of aluminum alloy stiffened sheet after friction stir welding by numerical simulation, Mater. Des. 32 (2011) 2284–2291. https://doi.org/10.1016/j.matdes.2010.11.032.

[22] Q.-Y. Shi, J. Silvanus, Y. Liu, D.-Y. Yan, H.-K. Li, Experimental study on distortion of Al-6013 plate after friction stir welding, Sci. Technol. Weld. Join. 13 (2008) 472–478. https://doi.org/10.1179/174329308X341924.

[23] K. Kuykendall, T. Nelson, C. Sorensen, On the selection of constitutive laws used in modeling friction stir welding, Int. J. Mach. Tools Manuf. 74 (2013) 74–85. https://doi.org/10.1016/j.ijmachtools.2013.07.004.

[24] Z. Zhang, J.T. Chen, The simulation of material behaviors in friction stir welding process by using rate-dependent constitutive model, J. Mater. Sci. 43 (2008) 222–232.

https://doi.org/10.1007/s10853-007-2129-1.

[25] P. Biswan, N.R. Mandal, Effect of Tool Geometries on ThermalHistory of FSW of AA110, Weld. J. 90 (2011) 129–135. https://app.aws.org/wj/supplement/wj201107_s129.pdf.

[26] R. Nandan, T. DebRoy, H.K.D.H. Bhadeshia, Recent advances in friction-stir welding – Process, weldment structure and properties, Prog. Mater. Sci. 53 (2008) 980–1023. https://doi.org/10.1016/j.pmatsci.2008.05.001.

[27] R. Nandan, G.G. Roy, T.J. Lienert, T. Debroy, Three-dimensional heat and material flow during friction stir welding of mild steel, Acta Mater. 55 (2007) 883–895. https://doi.org/10.1016/j.actamat.2006.09.009.

[28] R. Jain, S.K. Pal, S.B. Singh, A study on the variation of forces and temperature in a friction stir welding process: A finite element approach, J. Manuf. Process. 23 (2016) 278–286. https://doi.org/10.1016/j.jmapro.2016.04.008.

[29] T. Sheppard, D.S. Wright, Determination of flow stress: Part 1 constitutive equation for aluminium alloys at elevated temperatures, Met. Technol. 6 (1979) 215–223. https://doi.org/10.1179/030716979803276264.

[30] T. Sheppard, A. Jackson, Constitutive equations for use in prediction of flow stress during extrusion of aluminium alloys, Mater. Sci. Technol. 13 (1997) 203–209. https://doi.org/10.1179/026708397790302476.

[31] H. Schmidt, J. Hattel, A local model for the thermomechanical conditions in friction stir welding, Model. Simul. Mater. Sci. Eng. 13 (2005) 77–93. https://doi.org/10.1088/0965-0393/13/1/006.

[32] G. Buffa, J. Hua, R. Shivpuri, L. Fratini, A continuum based fem model for friction stir welding—model development, Mater. Sci. Eng. A. 419 (2006) 389–396. https://doi.org/10.1016/j.msea.2005.09.040.

[33] P. Heurtier, M.J. Jones, C. Desrayaud, J.H. Driver, F. Montheillet, D. Allehaux, Mechanical and thermal modelling of Friction Stir Welding, J. Mater. Process. Technol. 171 (2006) 348–357. https://doi.org/10.1016/j.jmatprotec.2005.07.014.

[34] H. Su, C.S. Wu, A. Pittner, M. Rethmeier, Thermal energy generation and distribution in friction stir welding of aluminum alloys, Energy. 77 (2014) 720–731. https://doi.org/10.1016/j.energy.2014.09.045.

[35] R.K. Uyyuru, S. V. Kailas, Numerical Analysis of Friction Stir Welding Process, J.

Mater. Eng. Perform. 15 (2006) 505–518. https://doi.org/10.1361/105994906X136070.

[36] J. Tang, Y. Shen, Numerical simulation and experimental investigation of friction stir lap welding between aluminum alloys AA2024 and AA7075, J. Alloys Compd. 666 (2016) 493–500. https://doi.org/10.1016/j.jallcom.2016.01.138.

[37] P. Asadi, R.A. Mahdavinejad, S. Tutunchilar, Simulation and experimental investigation of FSP of AZ91 magnesium alloy, Mater. Sci. Eng. A. 528 (2011) 6469–6477. https://doi.org/10.1016/j.msea.2011.05.035.

[38] S. Tutunchilar, M. Haghpanahi, M.K. Besharati Givi, P. Asadi, P. Bahemmat, Simulation of material flow in friction stir processing of a cast Al–Si alloy, Mater. Des. 40 (2012) 415–426. https://doi.org/10.1016/j.matdes.2012.04.001.

[39] G. Buffa, J. Hua, R. Shivpuri, L. Fratini, Design of the friction stir welding tool using the continuum based FEM model, Mater. Sci. Eng. A. 419 (2006) 381–388. https://doi.org/10.1016/j.msea.2005.09.041.

[40] R. Jain, S.K. Pal, S.B. Singh, Finite element simulation of pin shape influence on material flow, forces in friction stir welding, Int. J. Adv. Manuf. Technol. 94 (2018) 1781–1797. https://doi.org/10.1007/s00170-017-0215-3.

[41] L. Fratini, G. Buffa, L. Lo Monaco, Improved FE model for simulation of friction stir welding of different materials, Sci. Technol. Weld. Join. 15 (2010) 199–207. https://doi.org/10.1179/136217110X12665048207575.

[42] G. Buffa, D. Baffari, A. Di Caro, L. Fratini, Friction stir welding of dissimilar aluminium–magnesium joints: sheet mutual position effects, Sci. Technol. Weld. Join. 20 (2015) 271–279. https://doi.org/10.1179/1362171815Y.0000000016.

[43] G. Buffa, L. Fratini, Friction stir welding of steels: process design through continuum based FEM model, Sci. Technol. Weld. Join. 14 (2009) 239–246. https://doi.org/10.1179/136217109X421328.

[44] P. Asadi, M.K. Besharati Givi, M. Akbari, Simulation of dynamic recrystallization process during friction stir welding of AZ91 magnesium alloy, Int. J. Adv. Manuf. Technol. 83 (2016) 301–311. https://doi.org/10.1007/s00170-015-7595-z.

[45] A. Priyadarshini, S.K. Pal, A.K. Samantaray, Finite Element Modeling of Chip Formation in Orthogonal Machining, in: Stat. Comput. Tech. Manuf., Springer Berlin Heidelberg, Berlin, Heidelberg, 2012: pp. 101–144. https://doi.org/10.1007/978-3-

642-25859-6_3.

[46] A. Arora, M. Mehta, A. De, T. DebRoy, Load bearing capacity of tool pin during friction stir welding, Int. J. Adv. Manuf. Technol. 61 (2012) 911–920. https://doi.org/10.1007/s00170-011-3759-7.

[47] A. Arora, R. Nandan, A.P. Reynolds, T. DebRoy, Torque, power requirement and stir zone geometry in friction stir welding through modeling and experiments, Scr. Mater. 60 (2009) 13–16. https://doi.org/10.1016/j.scriptamat.2008.08.015.

[48] H.W. Zhang, Z. Zhang, J.T. Chen, 3D modeling of material flow in friction stir welding under different process parameters, J. Mater. Process. Technol. 183 (2007) 62–70. https://doi.org/10.1016/j.jmatprotec.2006.09.027.

[49] Z. Zhang, H.W. Zhang, Numerical studies on the effect of transverse speed in friction stir welding, Mater. Des. 30 (2009) 900–907. https://doi.org/10.1016/j.matdes.2008.05.029.

[50] J.W. Yoon, G.H. Bray, R.A.F. Valente, T.E.R. Childs, Buckling analysis for an integrally stiffened panel structure with a friction stir weld, Thin-Walled Struct. 47 (2009) 1608–1622. https://doi.org/10.1016/j.tws.2009.05.003.

[51] J.F. Caseiro, R.A.F. Valente, A. Andrade-Campos, J.W. Yoon, Elasto-plastic buckling of integrally stiffened panels (ISP): An optimization approach for the design of cross-section profiles, Thin-Walled Struct. 49 (2011) 864–873. https://doi.org/10.1016/j.tws.2011.02.011.

[52] C. Lynch, A. Murphy, M. Price, A. Gibson, The computational post buckling analysis of fuselage stiffened panels loaded in compression, Thin-Walled Struct. 42 (2004) 1445–1464. https://doi.org/10.1016/j.tws.2004.04.002.

[53] R.M.F. Paulo, Numerical simulation of the behaviour of reinforced structures, University of Aveiro, 2011.

[54] Y. Zha, T. Moan, Ultimate strength of stiffened aluminium panels with predominantly torsional failure modes, Thin-Walled Struct. 39 (2001) 631–648. https://doi.org/10.1016/S0263-8231(01)00027-1.

[55] M.R. Khedmati, A. Bayatfar, P. Rigo, Post-buckling behaviour and strength of multi-stiffened aluminium panels under combined axial compression and lateral pressure, Mar. Struct. 23 (2010) 39–66. https://doi.org/10.1016/j.marstruc.2009.10.003.

[56] M.R. Khedmati, M.R. Zareei, P. Rigo, Sensitivity analysis on the elastic buckling and

ultimate strength of continuous stiffened aluminium plates under combined in-plane compression and lateral pressure, Thin-Walled Struct. 47 (2009) 1232–1245. https://doi.org/10.1016/j.tws.2009.04.010.

[57] J.K. Paik, J.K. Seo, Nonlinear finite element method models for ultimate strength analysis of steel stiffened-plate structures under combined biaxial compression and lateral pressure actions—Part II: Stiffened panels, Thin-Walled Struct. 47 (2009) 998–1007. https://doi.org/10.1016/j.tws.2008.08.006.

[58] P. Rigo, R. Sarghiuta, S. Estefen, E. Lehmann, S.. Otelea, I. Pasqualino, B.. Simonsen, Z. Wan, T. Yao, Sensitivity analysis on ultimate strength of aluminium stiffened panels, Mar. Struct. 16 (2003) 437–468. https://doi.org/10.1016/j.marstruc.2003.09.002.

[59] R.M.F. Paulo, P. Carlone, V. Paradiso, R.A.F. Valente, F. Teixeira-Dias, Prediction of friction stir welding effects on AA2024-T3 plates and stiffened panels using a shell-based finite element model, Thin-Walled Struct. 120 (2017) 297–306. https://doi.org/10.1016/j.tws.2017.09.009.

[60] R.M.F. Paulo, P. Carlone, R.A.F. Valente, F. Teixeira-Dias, F. Rubino, Numerical simulation of the buckling behaviour of stiffened panels: Benchmarks for assessment of distinct modelling strategies, Int. J. Mech. Sci. 157–158 (2019) 439–445. https://doi.org/10.1016/j.ijmecsci.2019.04.042.

[61] J.F. Caseiro, R.A.F. Valente, A. Andrade-Campos, J.W. Yoon, On the elasto-plastic buckling of Integrally Stiffened Panels (ISP) joined by Friction Stir Welding (FSW): Numerical simulation and optimization algorithms, Int. J. Mech. Sci. 76 (2013) 49–59. https://doi.org/10.1016/j.ijmecsci.2013.09.002.

[62] J.K. Paik, A. Duran, Ultimate strength of aluminium plates and stiffened panels for marine applications, Mar. Technol. 41 (2004) 108–121.

[63] R.M.F. Paulo, F. Teixeira-Dias, R.A.F. Valente, Numerical simulation of aluminium stiffened panels subjected to axial compression: Sensitivity analyses to initial geometrical imperfections and material properties, Thin-Walled Struct. 62 (2013) 65–74. https://doi.org/10.1016/j.tws.2012.07.024.

[64] M.R. Khedmati, K. Ghavami, A numerical assessment of the buckling/ultimate strength characteristics of stiffened aluminium plates with fixed/floating transverse frames, Thin-Walled Struct. 47 (2009) 1373–1386.

https://doi.org/10.1016/j.tws.2009.03.008.

[65] M.R. Khedmati, M. Pedram, A numerical investigation into the effects of slamming impulsive loads on the elastic–plastic response of imperfect stiffened aluminium plates, Thin-Walled Struct. 76 (2014) 118–144. https://doi.org/10.1016/j.tws.2013.10.016.

[66] S. Benson, J. Downes, R.S. Dow, Load shortening characteristics of marine grade aluminium alloy plates in longitudinal compression, Thin-Walled Struct. 70 (2013) 19–32. https://doi.org/10.1016/j.tws.2013.04.006.

[67] R. Wilson, A. Murphy, M.A. Price, C. Glazebrook, A preliminary structural design procedure for laser beam welded airframe stiffened panels, Thin-Walled Struct. 55 (2012) 37–50. https://doi.org/10.1016/j.tws.2012.03.003.

[68] A. Murphy, T. Ekmekyapar, D. Quinn, M. Özakça, K. Poston, G. Moore, J. Niblock, The influence of assembly friction stir weld location on wing panel static strength, Thin-Walled Struct. 76 (2014) 56–64. https://doi.org/10.1016/j.tws.2013.11.004.

[69] P. Carlone, G.S. Palazzo, Influence of Process Parameters on Microstructure and Mechanical Properties in AA2024-T3 Friction Stir Welding, Metallogr. Microstruct. Anal. 2 (2013) 213–222. https://doi.org/10.1007/s13632-013-0078-4.

[70] R.M.F. Paulo, P. Carlone, R.A.F. Valente, F. Teixeira-Dias, G.S. Palazzo, Influence of friction stir welding residual stresses on the compressive strength of aluminium alloy plates, Thin-Walled Struct. 74 (2014) 184–190. https://doi.org/10.1016/j.tws.2013.09.012.

[71] M.R. Sonne, C.C. Tutum, J.H. Hattel, A. Simar, B. de Meester, The effect of hardening laws and thermal softening on modeling residual stresses in FSW of aluminum alloy 2024-T3, J. Mater. Process. Technol. 213 (2013) 477–486. https://doi.org/10.1016/j.jmatprotec.2012.11.001.

[72] Simulia Dassault Systémes, ABAQUS v.6.14, Abaqus Documentation, (2014). https://www.3ds.com/products-services/simulia/services-support/support/documentation/.

[73] A. Murphy, M. Price, R. Curran, P. Wang, Integration of Strength and Process Modeling of Friction-Stir-Welded Fuselage Panels, J. Aerosp. Comput. Information, Commun. 3 (2006) 159–176. https://doi.org/10.2514/1.17694.

[74] C.S. Smith, P.C. Davidson, J.C. Champman, P.J. Dowling, Strenght and stiffness of

ship's plating under in-plane compression and tension, R. Inst. Nav. Archit. Trans. (1987) 277–296. http://worldcat.org/issn/00358967.

[75] J.K. Paik, A.K. Thayamballi, J.Y. Ryu, J.H. Jang, J.K. Seo, S.W. Park, S.K. Seo, C. Renaud, H.P. Cojeen, N.I. Kim, The statistics of weld induced inicial imperfections in aluminium stiffened plate structures for marine applications, International Journal of Maritime Engineering, Trans. R. Inst. Nav. Archit. Part A Int. J. Marit. Eng. 148 (2006) 19–62.

[76] A. Murphy, M. Price, C. Lynch, A. Gibson, The computational post-buckling analysis of fuselage stiffened panels loaded in shear, Thin-Walled Struct. 43 (2005) 1455–1474. https://doi.org/10.1016/j.tws.2005.03.010.

APPENDIX A: Summary of the simplified methodology

The use of a simplified methodology to include the welding effects follows the examples available in the literature [1,52,56,65,66,68,73–76]. The magnitudes of the welding effects and their location on the panels were based on the FSW numerical analyses, although being added to the model with simplified distributions.

The yield stress distribution was modelled based on an approximation to the results of the FSW analyses. Two areas with different yield stress distributions were defined from the FSW analyses, as represented in Figure A1(a): one with the affected material properties (close to the weld line, with 12 mm width), and another with the base material properties (in the remaining area), The affected material was modelled with yield stress values corresponding to the material before (205 MPa) or after (259 MPa) ageing process, as shown in Figure A1(b). The picture shows the T profile, but the same approach was also applied to the analysis of B45 and B60 ones.

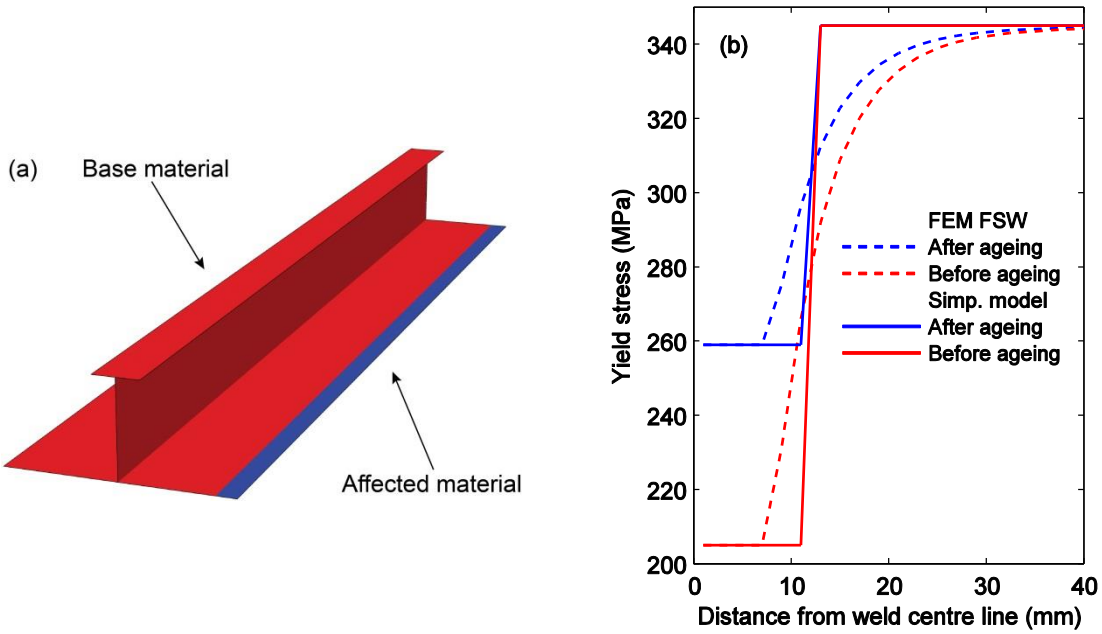

Figure A1: Distribution of the affected material in the simplified model: (a) full panel, and (b) along the mid-length section (the plot compares the simplified modelling approach against the distribution obtained from the FSW analyses).

The longitudinal stress was included in the model with a magnitude of 183 MPa in the zone close the weld line (with 14 mm width), as represented in Figure A2(a). For equilibrium

reason, a longitudinal compressive stress was applied in the remaining area of the panels. The magnitude of this compressive stress was calculated for each cross-section geometry, being applied with the absolute magnitudes of 15.96 MPa, 14.72 MPa and 12.91MPa, for panels B45, B60 and T, respectively. In the simplified modelling the added stress distribution was assumed constant across the thickness. This methodology required a relaxation step after the stress input, performed using only rigid body movement constrains, to take into account the typical distortion occurring after the FSW process (Figures A2(b-d)).

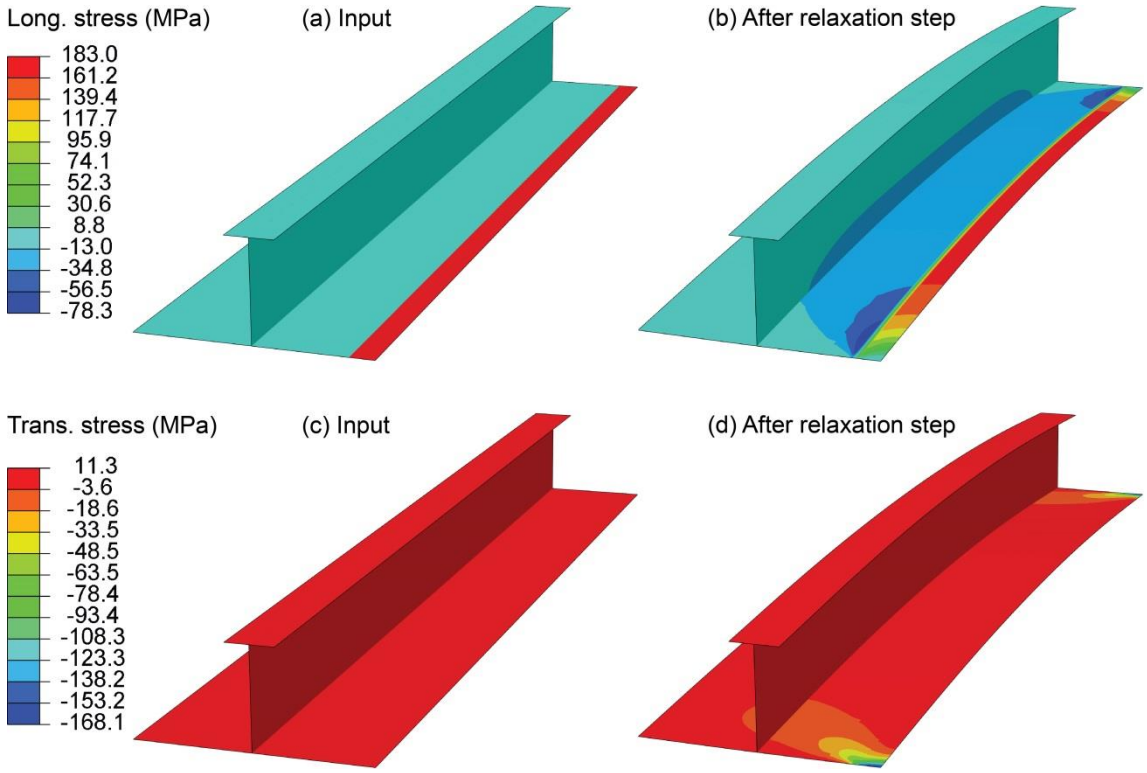

Figure A2: Longitudinal stress distribution in the panel T: (a) as inputted in the simplified model and (b) after the relaxation step; and transverse stress distribution: (c) as inputted in the simplified model and (d) after the relaxation step.

The relaxation step led to variations in final stress distributions for both longitudinal and transverse stresses (figure A2). Figure A3 shows longitudinal stress distribution in the panel mid-length as inputted, after the relaxation step and compared to the one obtained from the FSW analyses.

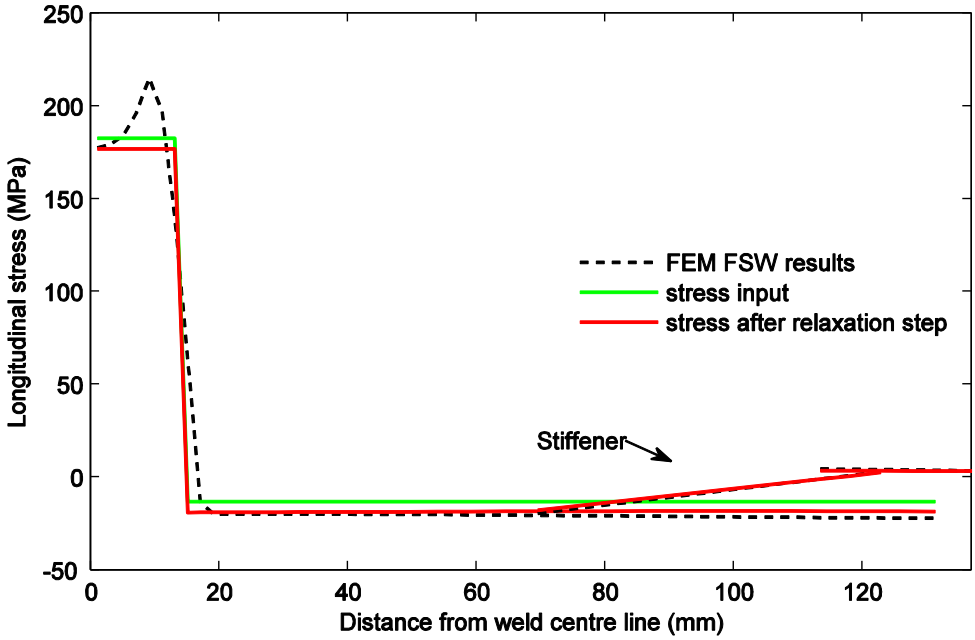

Figure A3: Longitudinal stress distribution in the mid–length section of panel T (average across thickness): as inputted in the simplified model and after the relaxation step, compared with the results from the FSW simulation.

Transverse stresses were not added to the model (Figure A2(c)) , although the relaxation step led to the increase of the transverse stress field, with a higher magnitude close to the longitudinal ends and the weld line, as can be seen in Figure A2(d). This distribution was similar to the one obtained from the welding analyses, albeit with lower magnitudes [59]. Figure A4 and A5 show the deformed shape and the relative displacements in the weld line after the relaxation step.

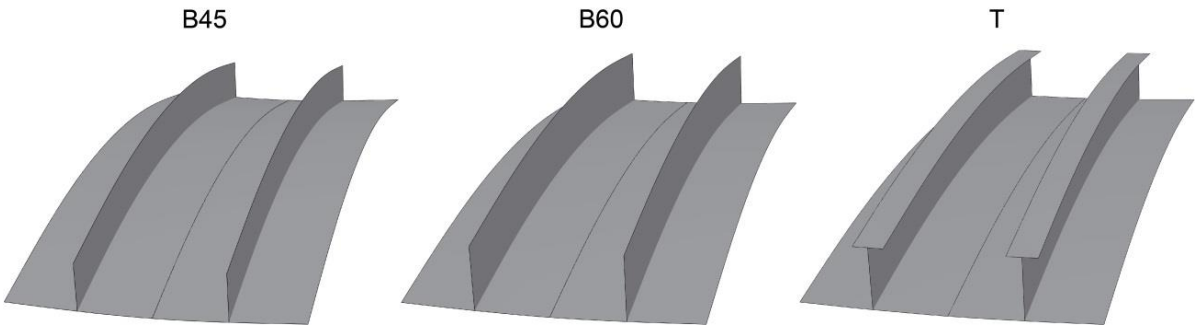

Figure A4: Deformed shapes obtained after the relaxation step (mirror view on the weld line symmetry plane and the displacements amplified 50 times along Oy).

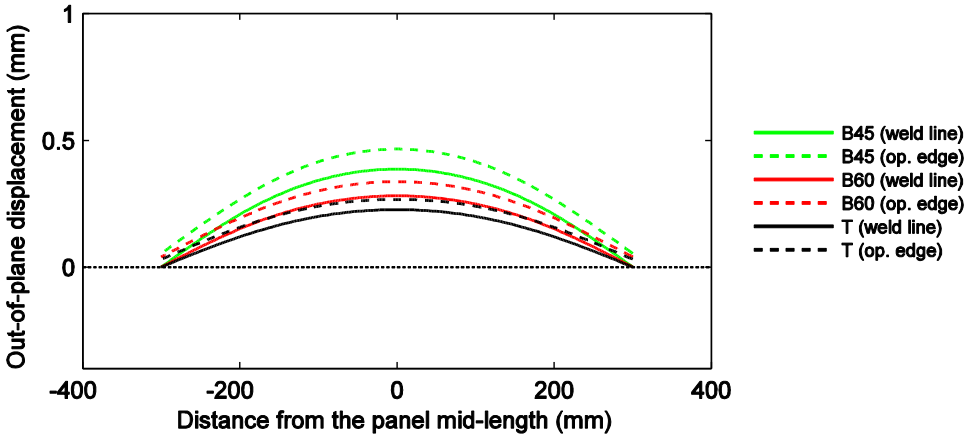

Figure A5: Displacement after the relaxation step along the weld line and opposite edge.

It should also be mentioned that the use of different softening magnitudes did not influence the results after the relaxation step, in terms of the finals stress or displacement distributions, since the stress field magnitude was lower that the yield stress in all tested cases.

APPENDIX B: Analysis of buckling shape evolution for the different panels

This appendix intends to provide an overall description of the buckling behavior of each panel, and therefore is focused on the evolution (and sensitivity) of each numerical model to the compressive loads/displacement, from a structural stability standpoint.

Starting with panels with the B45 cross section profile, Figure B1(a) shows the buckling behaviour as coming from the numerical models, for a given combination of geometric imperfections together with a softening model. It can be seen that the buckling mode evolves from a single curve to three half waves in the plate and stiffener, which lead to the collapse of the structure. In Figure B1(b), the spatial disposition of the subpictures relates to the model setup shown in Figure 2, regarding boundary conditions and reference axes.

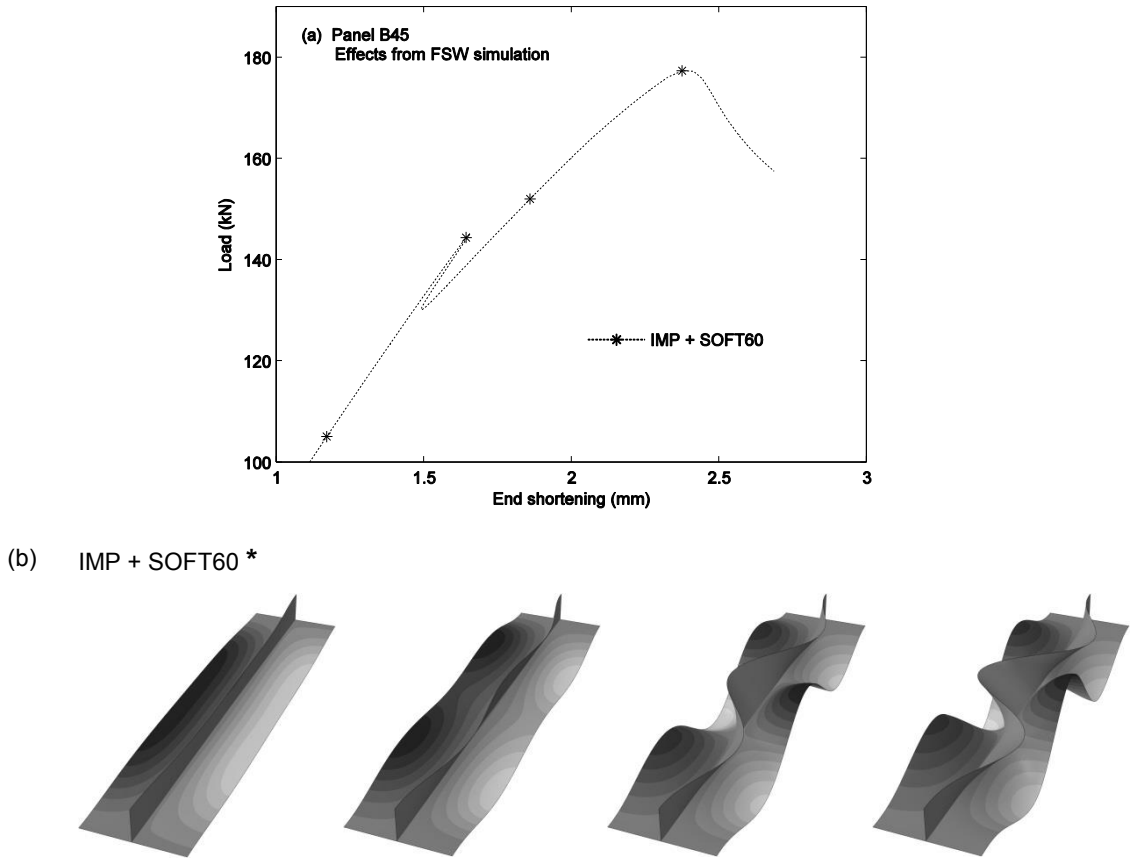

Figure B1: (a) Load/end shortening curves and (b) corresponding buckling modes obtained with panel B45 (displacements amplified 15 times along Ox and Oy).

Figure B2(a) shows the evolution of B60 panels with the load/displacement imposition, including the effects from FSW simulation and from the simplified modelling (Appendix A). The panels with the effects from the FSW simulation show a buckling evolution similar to the one presented by the panel B45 model (Figure B2(b)). The panels with the simplified modelling of the welding effects follow a similar evolution, albeit symmetric (Figure B2(c)), which reflects the influence of initial geometrical imperfections on the deformed configurations.

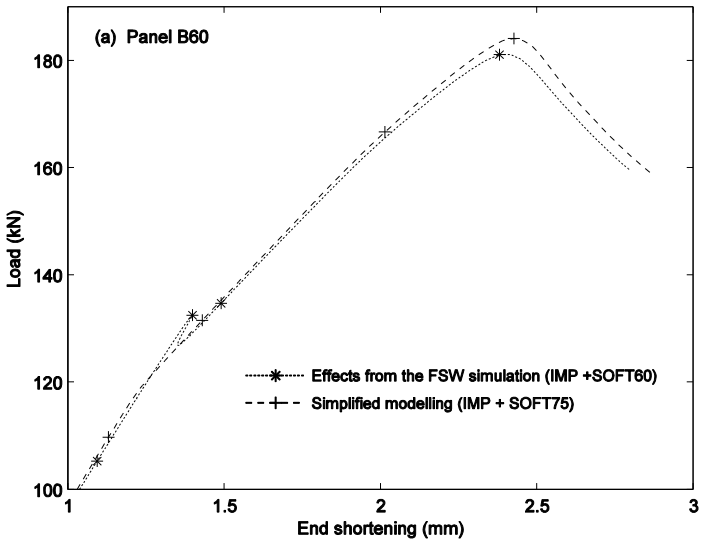

(b) Effects from the FSW simulation (IMP + SOFT60) *

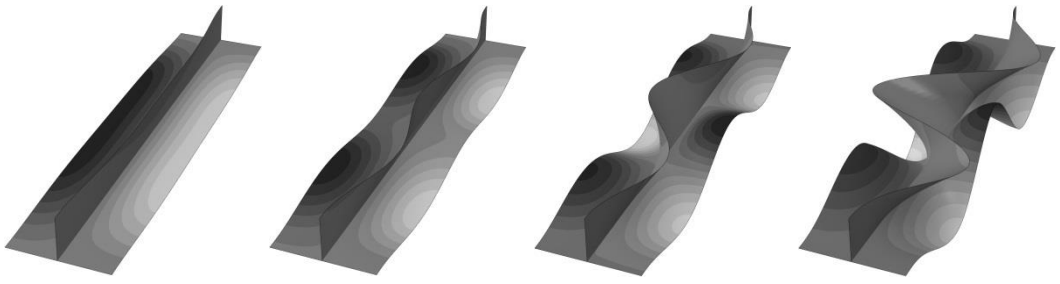

(c) Simplified modelling (IMP + SOFT75) +

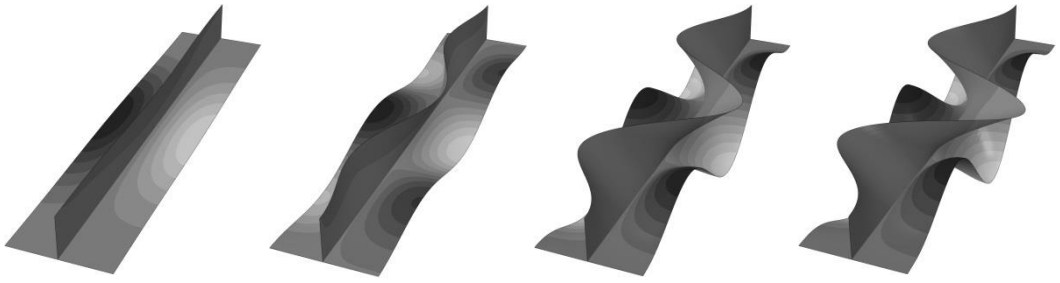

Figure B2: (a) Load/end shortening curves; (b) and (c) corresponding buckling modes obtained with panel B60 (displacements amplified 15 times along Ox and Oy).

Finally, for panel T (Figure B3(a)) four distinct buckling shape evolutions are observed. For the model with welding effects from the FSW simulation, shape evolutions associated with all the panels without and with residual stresses are represented in Figure B3(b) and B3(c), respectively. In this first case, the stiffener buckles in a single half wave. The plate buckled in a mode that combines five half waves with a single global curve induced by the stiffener displacement. This collapse can be associated to a mode-change behaviour, with the panel failing due to localised buckling, close to one of the transverse edges. For the panel T model, but including the residual stress field, a different buckling evolution can be seen (Figure B3(c)). The stiffener also buckles in a single global curve, but the localised buckle close to the transverse edge starts earlier than in panels without residual stresses, leading to lower collapse loads. In this case the mode-change was not associated with the collapse. Finally, the results for panel T using a simplified modelling approach (Appendix A) of the welding effects show a distinct buckling evolution, since the modelling simplifications lead to buckling shapes with symmetry considering the mid-length plane of the panel. Most of the panel T models exhibit a buckling shape evolution as shown in Figure B3(e). The stiffener buckles in a single global curve and the panel in a more complex shape. The only exception to this behaviour was observed with the model including only geometrical imperfections (IMP). In this case, the stiffener showed small out-of-plane displacements and the plate evolves from a single global curve to a three half waves shape and, later, to a five half waves shape, ultimately leading to collapse (Figure B3(e)).

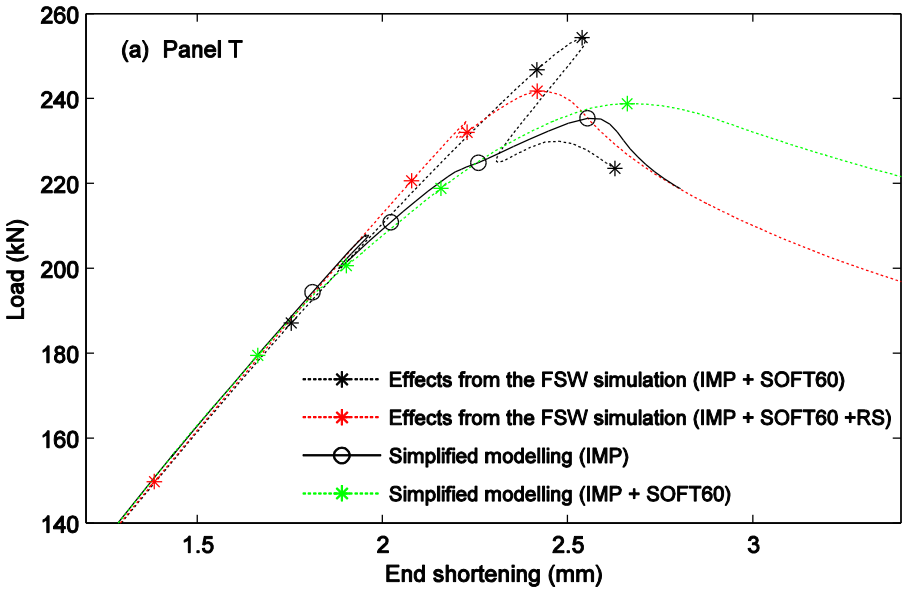

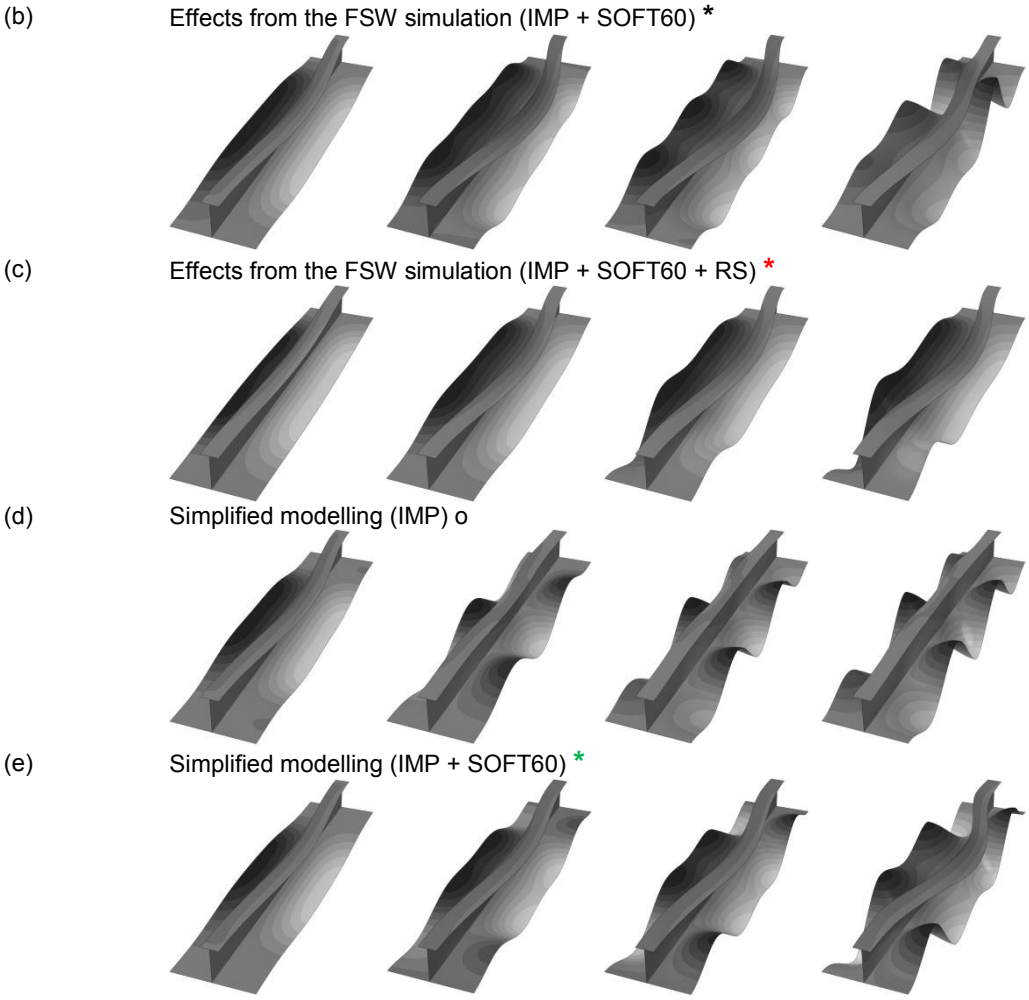

Figure B3: (a) Load/end shortening curves; (b), (c), (d) and (e) corresponding buckling modes obtained with panel T (displacements amplified 15 times along Ox and Oy).